Biosensors and Bioelectronics 41 (2013) 602–607

Contents lists available at SciVerse ScienceDirect

Biosensors and Bioelectronics

journal homepage: www.elsevier.com/locate/bios

Multifunctional microelectrode array (mMEA) chip for neural-electrical and neural-chemical interfaces: Characterization of comb interdigitated electrode towards dopamine detection

Min-Chieh Chuang [a,b], Hsin-Yi Lai [c], Ja-an Annie Ho [a,*], You-Yin Chen [d,**]

[a] Department of Biochemical Science and Technology, National Taiwan University, Taipei 10617, Taiwan
[b] Department of Chemistry, Tunghai University, Taichung 40704, Taiwan
[c] Department of Neurology, University of North Carolina, Chapel Hill, NC 27599, USA
[d] Department of Biomedical Engineering, National Yang Ming University, Taipei 11221, Taiwan

ARTICLE INFO

Article history:
Received 25 July 2012
Received in revised form
14 September 2012
Accepted 20 September 2012
Available online 28 September 2012

Keywords:
Neural chip
Microelectrode array
Interdigitated electrode
Electrochemical biosensor
Dopamine

ABSTRACT

Microelectrode array platforms have attracted considerable interest owing to their ability to facilitate interactive communications between investigators and neuronal network. We herein present an integrated multifunctional microelectrode array (mMEA) chip harnessed with multiple measurement modalities of both neural-electrical and neural-chemical recordings to enable simultaneous monitoring of action potential and the level of the specific neurotransmitter. A dopamine sensor modality fabricated in interdigitated electrodes (IDE) fashion was realized and characterized, subsequently applied to trace dopamine exocytosis in PC12 cells cultured on such mMEA chip. Facile fabrication process leveraging electroplating technique to implement the regulation of gap width was investigated and resulted in preferred IDE configuration. Collection efficiency and amplification effect were systematically evaluated. The as-fabricated sensing device exhibited a favorable diffusion-determining behavior reflected by the steady state current output, and in virtue of this feature, to detect dopamine in connection with limit of detection at 0.62 μM. The current signal was observed linear against the level of dopamine over the investigated concentration range with a resulting sensitivity of 0.096 nA μM^{-1}.

1. Introduction

In light of the growing senior population worldwide, neurological disorders, diseases favorably affecting the brain and nervous system of elderly, have attracted tremendous attention in recent years (Evans and Castleden, 1998; Snijders et al., 2007; Syrjälä et al., 2003). More than 50 million people are diagnosed with neurological disorders each year (Patel et al., 2007; Saleem et al., 2007). Since neurological disorders have complicated human health considerably, preventions and therapeutic protocols associated with these diseases are essentially demanded.

To address this requirement, a substantial body of work on various aspects of neuroscience researches has been implemented to develop advanced treatments and prevention strategies (Khansari and Coyne, 2012; Price et al., 2011). Of the developments, cultured (dissociated) neuronal network, a cell culture of neurons which is utilized as a model to study the central nervous system has been documented to be an invaluable tool to investigate the underlying principles behind neuronal learning, memory, connectivity, plasticity, and information processing (Charkhkar et al., 2012; Kiyohara et al., 2011). However, the acquired information remains insufficient to reconstitute the neural network systematically.

Typically cultured neuronal networks are connected to a device such as a multi-electrode array (MEA), thus allowing two-way communication between the investigators and the network. The spikes from the different sites of the neural network could be synchronously recorded enabling the researcher to pick up the temporal-spatial information for neural coding. While the recording of electrical signals could be achieved via the successful realizations of MEA-based neural chip, proper attention must be paid to integrate electrical signals with responses acquired from a great number of biochemical substances that lead to a better understanding of neuronal networks.

Dopamine (DA), a simple compound cataloged to the catecholamine family, has been identified as one of the significant neurotransmitters that directly relate to mental health problem. Distinct dysfunctions of the nervous system are associated with shortage (e.g., pakinson's disease) (Lewis and Barker, 2009) or excess (schizophrenia) (Gunduz-Bruce, 2009) of dopamine. This necessitates

* Corresponding author. Tel.: +886 2 3366 4439; fax: +886 2 3366 4438.
** Corresponding author. Department of Biomedical Engineering, National Yang Ming University, No.155, Section 2, Linong St.,Taipei, 11221 Taiwan. Tel.: +886 2 2826 7022; fax: +886 2 2608 0963.
E-mail addresses: jaho@ntu.edu.tw (J.-a. Annie Ho), irradiance@so-net.net.tw (Y.-Y. Chen).

0956-5663/$ - see front matter © 2012 Elsevier B.V. All rights reserved.
http://dx.doi.org/10.1016/j.bios.2012.09.030

a development of reliable and accurate dopamine monitoring systems. Such monitoring devices are also of considerable interest for drug discovery applications (Chen et al., 2008; Cui et al., 2006). In light of the significances of dopamine and its detection, versatile assay methods have been exploited (Lindsay et al., 2007; Perry et al., 2009; Wang et al., 2004). A majority of detection methods relied on electrochemical and sampling coupled techniques. In connection to the former which took an advantage of facile oxidation of dopamine, and by this feature, enormous efforts were inevitably focused on the modification of electrodes aiming to effective enhancement on both sensitivity and selectivity. Also advanced functionalizations of electrodes allowed a simultaneous detection of multiple monoamines, realized by utilizing electrochemical voltammetry (Hadi and Rouhollahi, 2012; Sun et al., 2011; Wang, 2005).

High temporal and spatial resolutions are essentially required in an *in situ ex vivo* or *in vitro* monitoring of dopamine accommodated in a cultured (dissociated) neuronal network. While electrochemical technique has offered favorable temporal resolution, spatial issue was not resolved yet. Utilizing either carbon fiber as detection probe or microdialysis sampling has harnessed the detection to partially give spatial information; whereas they required sophisticated preparation and instrument. To conquer the limitations, a multifunctional microelectrode array (mMEA) chip was described in this article to allow simultaneous recordings of electrical and chemical signals that led to preferred temporal and spatial resolutions. To the best of our knowledge, this is the first sophisticated chip endowed with multiple recording modalities in electrical and biochemical fashions. The fabrication of chips leverages electroforming technique, a relatively cost-effective approach, to yield a microstructure facilitating both cell adhesion and neurochemical detection. Specifically, varying deposition time to regulate the microstructure of interdigitated electrodes (IDE) was implemented to result in a DA sensing utility. The sensing performances of as-fabricated chip were characterized. An excitatory exocytosis of DA was also monitored by the mMEA chip.

2. Materials and methods

2.1. Chemicals and reagents

Potassium phosphate monobasic (KH_2PO_4), potassium phosphate dibasic (K_2HPO_4), sodium chloride (NaCl), calcium chloride ($CaCl_2$), potassium chloride (KCl), magnesium sulfate ($MgSO_4$), ionomycin, 3,4-dihydroxy-L-phenylalanine (L-DOPA), HEPES, poly-L-lysine hydrochloride, and dopamine hydrochloride (DA) were obtained from Sigma-Aldrich (St. Louis, MO) and used as supplied. Sulfuric acid (H_2SO_4,) was purchased from Riedel-de Han. RPMI, fetal bovine serum, and horse serum were acquired from Invitrogen Corporation (Carlsbad, CA). Deionized water (>18 MΩ cm) from a Direct-Q system (Millipore, Billerica, MA) was used to prepare all aqueous solutions. Positive (EPG 512) and negative (THB-110N) photoresists were attained from Everlight Chemical Industrial Corp. (Taiwan) and JSR Co. Ltd. (Taiwan), respectively. Gold electroplating solution (Aurotek ST6S, Resound Technology Inc., Taiwan), platinum electroplating solution (PLATANEX, Tanaka Kikinzoku International Co., Ltd., Japan), polyimide (PI-2611, HD Microsystems, USA), chromium etchant (eSolv EG-201, Demand International Corp., Taiwan), and copper etchant (RTE-Cu29 WBL-B, Resound Tech. Inc., Taiwan) were used as supplied. Four inch glass wafer (B270) was purchased from Hongin Precision Glass Corp. Taiwan.

2.2. Fabrication of mMEA chips

AutoCAD (AutoCAD 2002, Autodesk Inc., USA) was used to design the main elements of the mMEA chip: interconnecting tracks with connecter pads, comb interdigitated generator/collector electrodes (IDEs), microelectrodes (MEs), and ground electrodes (GEs). The specifications are illustrated in Table S1 with a resulting layout shown in Fig. S1.

Four masks were employed to the implementation of chip fabrication. The first mask (MASK #1) was used to construct the bases of the IDEs, MEs, GEs, and connecter pads along with the interconnecting tracks. The second mask (MASK #2) was employed to uncover the 60 units of electrodes (IDEs, MEs and GEs) and their corresponding connector pads from the polyimide passivation. The third mask (MASK #3) was used to construct the interdigitated collector electrodes. The last mask (MASK #4) configured the three-dimensional interdigitated generator electrodes and microelectrodes, and their corresponding connector pads.

Fabrication process was commenced by coating polyimide (60 μm in thickness) onto the glass wafer using a spin coater (Model KW-4A, CHEMAT Technology, Inc., Taiwan), followed by curing at 350 °C for 30 min in an inert gas oven (QHMO-2, CSUN MFG. Ltd., Taiwan). Chrome and copper thin films, 100 and 700 nm in thickness respectively, were deposited onto the polyimide layer as a conductive layer (Fig. S2A) by a sputter (Vvs-70L, VICTOR Taichung Machinery Works Corp., Ltd., Taiwan).

Subsequently MASK #1 was utilized to lithographically pattern the metal circuits, the 60 units of electrode bases (IDEs, MEs and GEs) along with their corresponding connector pad bases and the interconnecting tracks, followed by etching with chrome and copper etchants (Fig. S2B). Next, coating of a 3.2 μm-thick polyimide insulation layer was undertaken in which the layer was cured at 350 °C for 30 min in an inert gas oven. The 60 electrode/connector pad bases were uncovered afterward using O_2 plasma etching in connection to the utilization of MASK #2 to produce the pattern shown in Fig. S2C.

To construct the interdigitated collector electrodes with 6 electrode digits, Mask #3 was employed to create the layout. An electrodeposition of platinum on their corresponding Cu/Cr bases was subsequently implemented at 10 mA/cm^2 for desired period of time (Fig. S2D). The interdigitated generator electrodes were also generated by gold electroplating using Mask #4. Electroplating parameters were optimized to yield tailored IDE geometry (electrode thickness, surface area, electrode width and spacing) for a superior sensing performance. Lastly a 5 μm gold layer was deposited onto the ME and GE bases and all connector pads (Fig. S2E).

Prior to use, a glass ring (22 mm in inner diameter and 25 mm in outer diameter, 10 mm in height) was glued onto the mMEA chip using a silicon adhesive (Sylgard® 184 silicone elastomer kit, Dow Corning Corp., Midland, MI) to configure a miniaturized cell for following cell culture and electrochemical examinations.

2.3. Measurements and characterizations

Electrochemical measurements were performed at room temperature mostly using a 620A Electrochemical Analyzer (CH Instruments, Austin, TX); model CHI1030 was employed for carrying out the intra-assay to evaluate consistency of eight-unit IDEs. Either cyclic voltammetry (CV) or chronoamperometry was used to electrochemically characterize the IDE on the mMEA chip in a 50 mM phosphate buffer solution (pH 7.4). To facilitate the measurements, chips were situated horizontally on the bench and a 0.6 mL sample was pipetted onto the chip covering the IDE, as well as an external platinum wire and Ag/AgCl wire (both are 0.25 mm in diameter) as counter and reference electrodes, respectively. Scan rate applied in CV is 0.1 V/s. Chronoamperometric currents were sampled 180 s after the potential step. For an estimation of electrode area, cyclic voltammogram recorded in 0.1 M sulfuric acid solution, using the similar three-electrode configuration above, was observed. The area of the gold oxide reduction peak was converted to real electrode area, in virtue of

a two-electron reduction of Au (111) surface equal to 400 μC/cm^2. The morphology and profile of the electrode was examined using an optical microscope (Nikon SMZ1000, Tokyo, Japan) and an atomic force microscope (JPK NanoWizard, Berlin, Germany).

2.4. PC12 cell culture on the mMEA chip

The as-fabricated mMEA chips were autoclaved at 122 °C for 10 min, followed by 20 min of drying and cooling to the room temperature. To enhance the cell adhesion, mMEA chips were coated with 1 mL poly-L-lysine solution (100 mg/mL, equilibrated in phosphate buffer solution and stored at 4 °C) and stood for 60 min at room temperature. Subsequently the chips were quadruply cleaned with 1 mL deionized water and dried in a culture hood for 30 min.

Rat phaeochromocytoma cell, clone PC12, was utilized as the cellular model to study DA exocytosis on the chip. 5×10^6 cells in a 100 μL glucose Dulbecco's Modified Eagle Medium (DMEM) were seeded onto the mMEA chip with the growth medium (RPMI 1640 supplemented with 10% fetal bovine serum and 5% horse serum) and were grown in a humidified incubator at 37 °C with 5% CO_2. The medium was changed every 2 days. Cells grown to 80% confluence were transferred to a micro-incubation system (see Figs. S3–S5 for details) to expedite the study of DA exocytosis upon a potassium ion stimulation.

2.5. In situ examination of DA exocytosis

To monitor the dopamine secretion from PC12 cells, culture medium was removed from the mMEA chip and cells were washed twice with Locke-Ringer solution (10 mM HEPES, pH 7.2, 150 mM NaCl, 3 mM $CaCl_2$, 2 mM KCl, 1 mM $MgSO_4$). Subsequently the mMEA chip (containing PC12 cells) was allowed to equilibrate in Locke-Ringer solution with 100 μM L-DOPA for 1 h in the micro-incubator system (with 5% CO_2 atmosphere at 37 °C) upon receiving a fresh stimulation buffer containing 55 mM KCl and 5 μM ionomycin. Stimulation was executed by injecting 15 μL stimulation buffer using a syringe pump at the rate of 50 mL/h. Through whole stimulation route, amperometric technique was applied to record the current from the IDE to monitor the level of DA temporally. Potentials applied at generator electrode and collector electrodes were 0.5 V and −0.25 V (vs. Ag/AgCl) respectively.

3. Results and discussion

Similar to a conventional MEA chip utilized for the measurement of action potential, the mMEA chip exhibited central capability of electrophysiological recording (Figs. S6 and S7). However, the characterization of electrical recording from neuronal activities is not the main focus of this article and will be discussed in separate study.

Instead of the thin film technology incorporating the masks to yield patterned electrode with desired dimension, an electroplating technique was carried out, which is a relatively cost-effective approach to produce IDE with regulable gap width by controlling the deposition time. This thus drastically mitigated the applications of mask and lithographic development. An optical micrograph of the integrated mMEA neural chip is given in Fig. 1A, depicting a well-fabricated chip with a sampling cell constructed by a glass ring. Fig. 1B exhibits the central region of the chip revealing the layout of patterned arrays, comprising 40 MEs, 8 comb IDEs, and 4 GEs, as well as conductive tracks and pads made of gold. Further detailed illustration of IDE aiming for biochemical sensing is addressed in Fig. 1C where precisely fabricated IDE containing 6 pairs of digital electrodes (50 μm in length) are displayed. Highly reproducible fabrication of IDE and electrical recording electrodes were obtained.

To regulate gap width using the electroplating technique, an extended electroplating time leading to an exceeding deposition beyond the cavity volume was exerted. Fig. 2A depicts the envisaged deposition processes. Gold was electrodeposited into the cavity, created by the polyimide insulator (Fig. 2A (a)), to reach the stage shown as Fig. 2A (b). A prolonged deposition was subsequently conducted to drive deposit grow upward and sideward, yielding architectures as indicated in Fig. 2A (c) and (d), wherein the deposition exceeded the height of the cavity in connection with a progressive reduction of gap width of IDE.

A closer inspection of IDE was performed by atomic force microscopy with a resulting image shown in Fig. 2B. In line with the desired design, the length of individual comb electrode is 50 μm, along with varied gap width regulated by exceeding deposition approach. Fig. 2C illustrates the surface profile of two comb electrodes, sitting in proximity, along with a path designated with white arrow (in Fig. 2B), revealing a 5.7 μm of gap width and 1.4 μm of thickness exceeding the depth of cavity.

Table S2 summarizes the characterizations of as-fabricated mMEA chips (denoted as I, II, and III), given in connection to different deposition time. Chip I was produced with 15 min deposition time, resulting in the IDE at 10.5 μm gap width and 0.86 μm of maximum height (i.e., the thickness beyond the depth of cavity). Prolonged deposition time of 20 and 35 min led to the production of chip II and III, exhibiting gap width of 5.7 and 2.9 μm as well as maximum height of 1.41 and 3.75 μm, respectively. The resulting surface area of each generator electrode was estimated by integrating the electrochemical reduction peak area (in cyclic voltammogram), held in 0.1 M sulfuric acid, based on the factor of 400 μC/cm^2 (Abbott et al., 1994). As indicated in Table S2, chip III exhibited 4.65×10^{-5} cm^2 of

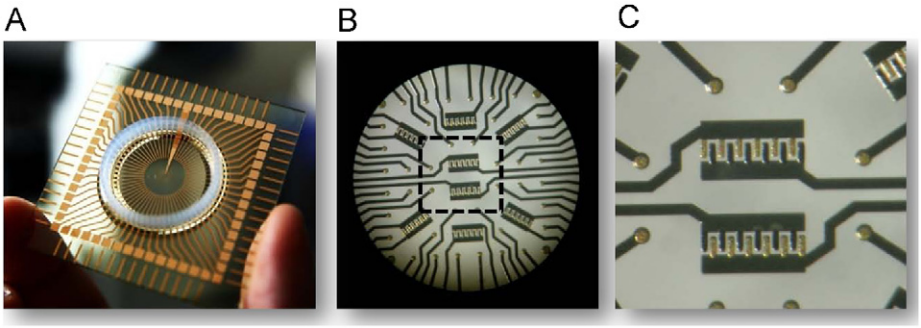

Fig. 1. (A) Optical micrographs of multifunctional multi-electrode array (mMEA) neural chip composing of 40 electrical recording sites, 8 comb interdigitated electrodes (IDE), and 4 ground ports; (B) magnified top-view images of the central part of the chip; and (C) magnified images of comb IDE containing gold generator and platinum collector finger electrodes. See text for the fabrication details.

surface area, higher than that of chip II (3.02×10^{-5} cm^2) and I (2.87×10^{-5} cm^2), in which good correlation was found between electrode area and the deposition time.

To characterize the electrocatalytic activity of the as-prepared IDE to the neural relevant substances and amplification effect brought by the utilization of collector electrode, cyclic voltammetric experiments of mMEA chips were conducted in a DA-containing solution. As illustrated in Fig. 3A, typical cyclic voltammograms with respect to 560 μM DA are attained in both single (a) and GC (i.e., dual electrodes mode incorporating a generator and a collector electrodes in IDE fashion) modes (b and c), in which sigmoidal shape of current curves are observed in both the generator and collector electrodes inferring a reachable steady state of the IDEs.

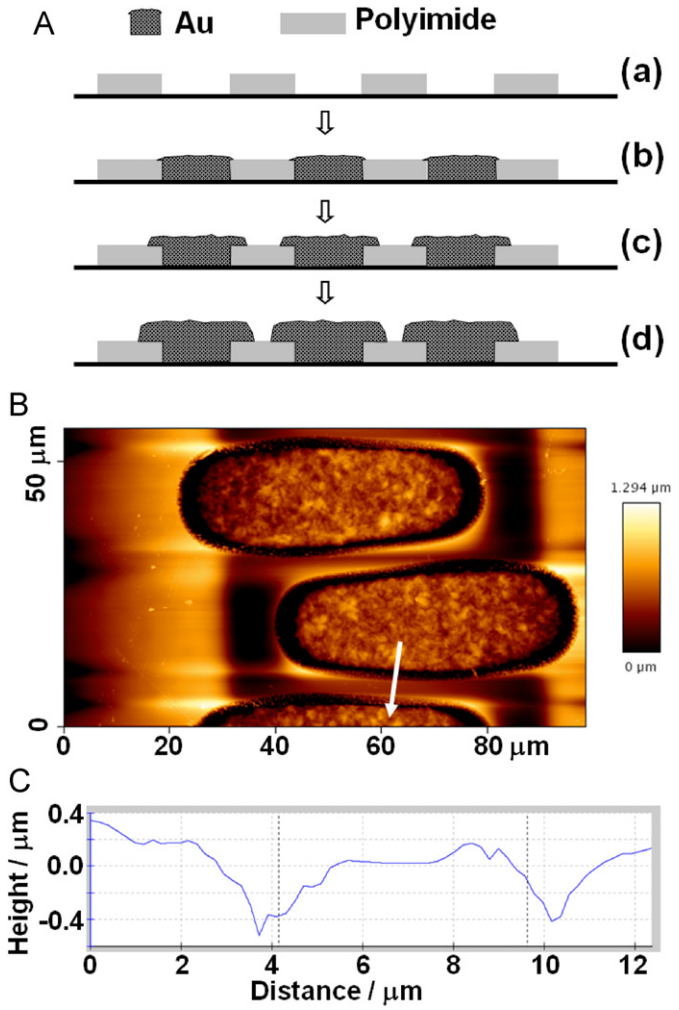

Fig. 2. (A) Envisaged deposition processes of (a) cavity created by polyimide, (b) deposition of gold (or platinum) in the cavity, (c) and (d) a prolonged deposition driving deposit grow upward and sideward; (B) a micrograph of IDE imaged by atomic force microscopy; and (C) corresponding surface profile along the white arrowed track (in B).

The steady state current (i_G) obtained from the generator electrode (60.8 nA, recorded at 0.6 V in curve b) was more than two fold higher than that (i_0) in the single electrode mode (29.6 nA in curve a), revealing the amplification effect caused by the utilization of collector electrode. Meanwhile the steady-state current at collector electrode (i_C) was approximately two third of i_G, attributed to the pseudo-reversibility of dopamine/quinolyl derivative and the potential escaping (away from the electrode) of the produced quinolyl derivative. i_G and i_C, as functions of sweep rate performed in cyclic voltammetry, were also evaluated (Fig. 3B). The currents were minimally dependent on the sweep rate in the given range. Furthermore, potential positioned for collector electrode (E_C) was also studied. Spanning E_C from −0.1 to −0.3 V (Fig. 3C), i_G and i_C increased between −0.1 and −0.2 V, subsequently alleviated to approximate constant at escalating potential. This reflected enhanced quantity of oxidized substances cycled by the collector electrode at increased overpotential; as well as a diffusion determining process at potential more negative than −0.2 V.

In a paradigm utilizing an electrode in the potential sweeping technique, the resulting maximum current at 25 °C is expressed as

$$i = i(\text{plane}) + i(\text{radial}) = 2.69\times10^5 n^{3/2} A D_0 \upsilon^{1/2} + 0.725 \times 10^5 n A D_0 C_0 / r_0 \quad (1)$$

where n, A, D_0, C_0, r_0, and υ are the number of electron transferred, the area of generator electrode in cm^2, the diffusion coefficient in cm^2/s, the concentration of DA in mol/cm^3, the radius of the generator electrode in cm^2, and the potential sweep rate in V/s, respectively. For the electrode with a radius size in micrometer (i.e., a microelectrode given with ultrasmall r_0), the i (radial) term dominates the current leading to a voltammogram in steady-state response independent of υ (illustrated in Fig. 3B). D is thus obtained to be 6.4×10^{-6} cm^2/s (on basis of the estimated real surface area shown in Table S2), in good agreement with those reported in previous literatures (Galal et al., 2012; Mazloum-Ardakani et al., 2009). This verified again the unique nature of microstructure of IDE in the mMEA chips operated in diffusion determining regime.

Defining the ratio of i_C and i_G (i_C/i_G) as collection efficiency (η) to evaluate the performance of IDE established among 3 chips were also summarized (Table 1). It was found that the increase

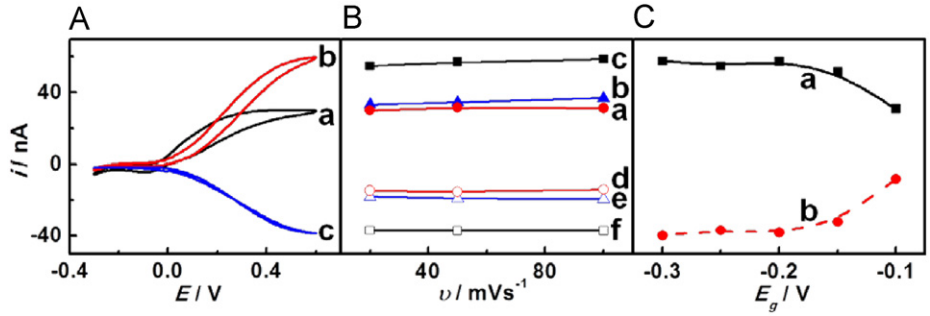

Fig. 3. (A) Cyclic voltammograms (CVs) recorded at (a) generator electrode operated in single electrode mode, as well as (b) generator electrode and (c) collector electrode operated in GC mode in a 560 μM dopamine solution measured in the potential ranging from −0.3 to 0.6 V (vs. Ag/AgCl) at 100 mV s^{-1}. Potential at collector electrode (E_C): −0.25 V. Effects of scan rate (B) and potential of collector electrode (C) upon the current. (a–c) in (B) and (a) in (C) are obtained from the generator electrode. (d–f) in (B) and (b) in (C) are recorded from the collector electrode.

Table 1
Electrochemical characterizations of mMEA chips operating in single electrode and GC modes.

Chip	Single mode	GC mode			
	Generator, i_0/nA	Generator, i_G/nA	Collector, i_C/nA	Collection efficiency, η/%	Amplification, Amp
I	22.8	30.0	15.0	50.0	1.31
II	26.1	37.4	20.1	53.7	1.43
III	29.6	60.8	40.0	66.0	2.05

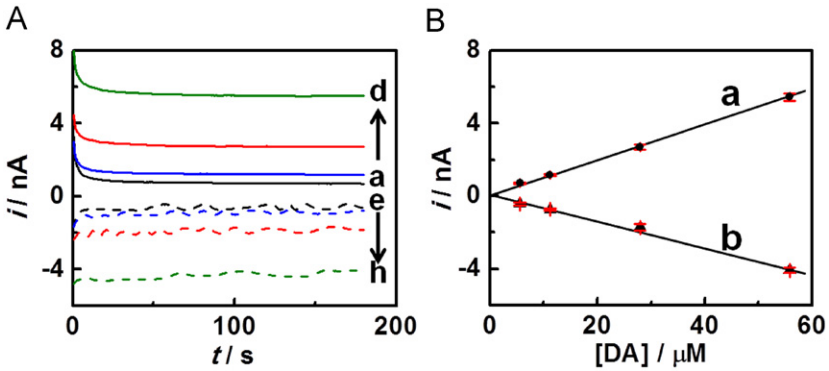

Fig. 4. (A) Chronoamperometric responses of generator electrode (a–d) and collector electrode (e–h) of the interdigitated electrode (chip III) to (a,e) 5.6, (b,f) 11.2, (c,g) 27.9, and (d,h) 55.8 μM of dopamine. (B) Corresponding calibration plots of the current recorded at the 180th s. The standard deviation are approximately 4–35 and 70–139 pA (dependent on DA concentration, $n=3$) at generator and collector electrodes, respectively. Potential at generator electrode: 0.5 V (a); collector electrode: −0.25 V (b) (vs. Ag/AgCl).

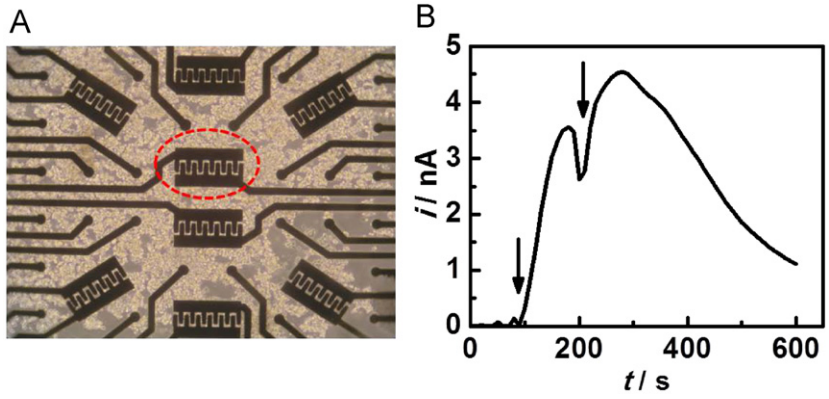

Fig. 5. (A) Optical micrographs of multifunctional multielectrode array (mMEA) neural chip cultured with PC12 cell. (B) Response curve recorded in an *in situ* measurement of dopamine exocytosis with potassium excitatory spike at the 95th and 205th second. The current is recorded from the IDE highlighted with red cycle in (A). Arrows in (B) denote the onset stimulated with a secretagogue (55 mM KCl and 5 μM ionomycin). Potential applied at generator electrode: 0.5 V; at collector electrode: −0.25 V (vs. Ag/AgCl). See text for the culture details. (For interpretation of the references to color in this figure legend, the reader is referred to the web version of this article.)

of η was significantly dependent upon the gap width, from 50 (chip I), 53.7 (chip II), to 66% (chip III). The increasing η is rationalized by the enhanced diffusion efficiency through the electrode gap (detailed in last paragraph of Supporting information). It was also worth mentioning that η observed in this study is higher than those reported by Ueno and co-workers (Ueno et al., 2003), in which maximum collection efficiency (50%) was obtained in a IDE with comparable length of electrode, demonstrating the relatively superior feature of the IDE prepared herein. While IDE given with greater number and longer length of comb electrodes are theoretically anticipated to offer higher collection efficiency, such a utility requires greater space to suit in, which is detrimental to the integration of mMEA chips. In addition, high density of fabrication requires higher class of microfabrication facility and instrument that substantially rises up the cost. This underlines a significance of desired electrode pattern suited in a limited space to preclude a crosstalk between separated sensor units, allowing accurate signal recording at both electrical stimulating and sensing sites.

Amplification factor (Amp) is another measure investigated in this study, defined as the ratio of currents acquired between GC (i_G) and single electrode (i_0) modes. Amp of three chips are indicated in Table 1 where chip III offers a value of 2.05, significantly higher than 1.43 (II) and 1.31 (I) in connection to varied gap width, as a result of enhanced diffusion efficiency through the electrode gap.

Chronoamperometric experiments, commonly performed for electrochemical sensing technology, were subsequently carried out to assess the sensing performance of the integrated mMEA chip. Fig. 4A depicts typical sensing curves recorded from the generator and collector electrodes (chip III) toward varied concentration of dopamine. Both generator and collector electrodes attained steady state current within a few seconds. Obviously the

current increased with elevated DA concentration, with a resulting calibration plot shown in Fig. 4B. The sensitivity is 0.096 nA μM^{-1} at the generator electrode. A reliable limit of detection (LOD) of the chip was also estimated by iterating the sensing examination until the current level was separated by three standard deviation (3σ) from background output. This corresponded to 0.62 μM of dopamine. The collection efficiencies for varied concentrations range 65–72%, slightly higher than those recorded by cyclic voltammetry.

Consistency of the 8 units of IDE sensing utilities was also characterized (Fig. S8). The result of intra-assay assessment for the chips indicated coefficient of variation for generator and collector electrode were 3.43 and 3.53%, respectively. Such results underscored the reproducible fabrication and the resulting capability of the IDE sensing devices, built in this novel integrated chip, could be favorably applied to the neuronal cell research for acquiring spatially profile cellular behavior by mitigating measurement variation.

For an ultimate use of this sensor utilized for *in vitro* cellular investigation, PC12 cell was cultured on the chip (Fig. 5A) to commence an *in situ* measurement of DA exocytosis induced by potassium chloride. The seeded cells (5×10^6 in a 100 μL) were grown and tested in the micro-incubation system at 37 °C with 5% CO_2. As can be interpreted from Fig. 5B, the IDE exhibits a speedy rising current upon a spike of the K^+ stimulation applied at the 95th and 205th second (as indicated by the arrows). PC12 cells are known as dopaminergic cells which contain catecholamine molecules and release dopamine upon the K^+ stimulation (Chen et al., 1994; Pothos et al., 1996). A background study conducted on a bare chip (i.e., without cells attached on the chip) was also implemented to confirm that the current was not increased by the K^+ injection. This proved that the mMEA was well-suited to offer spatial and real-time information brought from the multiple sensing units to learn cellular behavior cultured on the chip.

4. Conclusions

In conclusion, the work presented herein describes an integrated multifunctional microelectrode array chip and its flexible fabrication processes implemented by electroplating technique. This cost-effective, yet robust methodology is demonstrated to be well-suited for the formation of an interdigitated electrode sensing device with regulable gap width. The as-fabricated chips could be further extended to the demonstration of dopamine detection exhibiting reproducible and linear relationship of the steady state current signal against serial concentrations of dopamine, as well as a LOD down to 0.62 μM. Furthermore the chip demonstrated successful leveling of dopamine exocytosis of PC12 cell line upon stimulation with the potassium ion. The integration of both neural-electrical and neural-chemical recording modalities in the chip provides new opportunities to acquire neural network information temporally and spatially, consequently holds the potential for efficient and versatile analysis for studies in neuronal behavior and drug screening.

Acknowledgments

This work is supported by National Science Council Taiwan under Contracts 98-2113-M-002-025-MY3, 100-2113-M-002-016-MY2 and 100-2811-M-002-023.

Appendix A. Supporting information

Supplementary data associated with this article can be found in the online version at http://dx.doi.org/10.1016/j.bios.2012.09.030.

References

Abbott, N.L., Rolison, D.R., Whitesides, G.M., 1994. Langmuir 10, 2672–2682.
Charkhkar, H., Knaack, G.L., Gnade, B.E., Keefer, E.W., Pancrazio, J.J., 2012. Sensors and Actuators B: Chemical 161, 655–660.
Chen, T.K., Luo, G., Ewing, A.G., 1994. Analytical Chemistry 66, 3031–3035.
Chen, Y., Guo, C., Lim, L., Cheong, S., Zhang, Q., Tang, K., Reboud, J., 2008. Analytical Chemistry 80, 1133–1140.
Cui, H.F., Ye, J.S., Chen, Y., Chong, S.C., Liu, X., Lim, T.M., Sheu, F.S., 2006. Sensors and Actuators B: Chemical 115, 634–641.
Evans, S.N., Castleden, C.M., 1998. British Journal of Urology 82, 71–78.
Galal, A., Atta, N.F., El-Ads, E.H., 2012. Talanta 93, 264–273.
Gunduz-Bruce, H., 2009. Brain Research Reviews 60, 279–286.
Hadi, M., Rouhollahi, A., 2012. Analytica Chimica Acta 721, 55–60.
Khansari, P.S., Coyne, L., 2012. Inflammopharmacology 20, 159–167.
Kiyohara, A., Taguchi, T., Kudoh, S.N., 2011. IEEJ Transactions on Electrical and Electronic Engineering 6, 163–167.
Lewis, S.J.G., Barker, R.A., 2009. Journal of Clinical Neuroscience 16, 620–625.
Lindsay, S., Vázquez, T., Egatz-Gómez, A., Loyprasert, S., Garcia, A.A., Wang, J., 2007. Analyst 132, 412–416.
Mazloum-Ardakani, M., Beitollahi, H., Ganjipour, B., Naeimi, H., Nejati, M., 2009. Bioelectrochemistry 75, 1–8.
Patel, V., Simbine, A.P.F., Soares, I.C., Weiss, H.A., Wheeler, E., 2007. The Lancet 370, 1055–1060.
Perry, M., Li, Q., Kennedy, R.T., 2009. Analytica Chimica Acta 653, 1–22.
Pothos, E., Desmond, M., Sulzer, D., 1996. Journal of Neurochemistry 66, 629–636.
Price, A., Rayner, L., Okon-Rocha, E., Evans, A., Valsraj, K., Higginson, I.J., Hotopf, M., 2011. Journal of Neurology, Neurosurgery and Psychiatry 82, 914–923.
Saleem, T., Leigh, P.N., Higginson, I.J., 2007. Journal of Palliative Care 23, 291–299.
Snijders, A.H., Van De Warrenburg, B.P., Giladi, N., Bloem, B.R., 2007. The Lancet Neurology 6, 63–74.
Sun, C.L., Chang, C.T., Lee, H.H., Zhou, J., Wang, J., Sham, T.K., Pong, W.F., 2011. ACS Nano 5, 7788–7795.
Syrjälä, P., Luukinen, H., Pyhtinen, J., Tolonen, U., 2003. Journal of Neurology 250, 1063–1069.
Ueno, K., Kim, H.B., Kitamura, N., 2003. Analytical Chemistry 75, 2086–2091.
Wang, J., 2005. Electroanalysis 17, 7–14.
Wang, J., Chen, G., Chatrathi, M.P., Musameh, M., 2004. Analytical Chemistry 76, 298–302.